Energy and Buildings 158 (2018) 1429–1441

Contents lists available at ScienceDirect

Energy and Buildings

journal homepage: www.elsevier.com/locate/enbuild

Prediction of wind pressure coefficients on building surfaces using artificial neural networks

Facundo Bre[a,b,*], Juan M. Gimenez[a,c], Víctor D. Fachinotti[a]

[a] Centro de Investigación de Métodos Computacionales (CIMEC), UNL, CONICET, Predio "Dr. Alberto Cassano", Colectora Ruta Nacional 168 s/n, 3000 Santa Fe, Argentina
[b] Grupo de Investigación en Mecánica Computacional y Estructuras (GIMCE), Facultad Regional Concepción del Uruguay (FRCU), Universidad Tecnológica Nacional (UTN), 3260 Concepción del Uruguay, Argentina
[c] Facultad de Ingeniería y Ciencias Hídricas – Universidad Nacional del Litoral, Ciudad Universitaria, Paraje "El Pozo", Santa Fe, Argentina

ARTICLE INFO

Article history:
Received 28 July 2017
Received in revised form 3 November 2017
Accepted 21 November 2017
Available online 22 November 2017

Keywords:
Pressure coefficient
Natural ventilation
Building performance simulation
Artificial neural network

ABSTRACT

Knowing the pressure coefficient on building surfaces is important for the evaluation of wind loads and natural ventilation. The main objective of this paper is to present and to validate a computational modeling approach to accurately predict the mean wind pressure coefficient on the surfaces of flat-, gable- and hip-roofed rectangular buildings. This approach makes use of artificial neural network (ANN) to estimate the surface-average pressure coefficient for each wall and roof according to the building geometry and the wind angle. Three separate ANN models were developed, one for each roof type, and trained using an experimental database. Applied to a wide variety of buildings, the current ANN models were proved to be considerably more accurate than the commonly used parametric equations for the estimation of pressure coefficients. The proposed ANN-based methodology is as general and versatile as to be easily expanded to buildings with different shapes as well as to be coupled to building performance simulation and airflow network programs.

1. Introduction

Energy consumption and indoor environment of buildings are influenced by air infiltration and ventilation [1,2]. Wind induced pressure on the building envelope affects the air infiltrations because of the indoor–outdoor pressure difference. Wind pressure is also an important boundary condition for a wide range of problems, including heat, air and moisture (HAM) transfer, airflow network (AFN), and building energy simulation (BES) [3]. Generally, the wind pressure is characterized by the pressure coefficient defined as:

$$C_p = \frac{P_x - P_0}{\rho U_h^2/2},$$

where P_x is the static pressure at a given point on the building façade, P_0 is the static reference pressure at freestream, $\rho U_h^2/2$ is the dynamic pressure at freestream, ρ is the air density and U_h is the wind speed, which is often taken at the building height h in the upstream undisturbed flow.

A review of pressure coefficient data for building energy simulation and airflow network programs was made by Cóstola et al. [3]. They classified the sources of C_P data in two main groups: (i) primary sources, including full-scale measurements, reduced-scale wind-tunnel tests and computational fluid dynamics (CFD) simulations, and (ii) secondary sources, like databases and analytical models. Usually, because of their difficulty and cost, full-scale and wind-tunnel scale measurements are only used for the development of wind pressure coefficient databases or the evaluation of complex high-rise buildings. Analytical models are commonly used to predict surface-average C_P on low-rise buildings, where the variation of C_P over the surface can be neglected assuming that cracks are homogeneously distributed over the building façades [4]. This simplified approach is widely used to include airflow network analysis in BES [5].

Swami and Chandra [6] proposed simple equations for low- and high-rise buildings separately, which were obtained using stepwise regression analysis to fit some previously published studies of wind pressure coefficients. The Swami and Chandra's equation for low-rise buildings – from now on, referred to as the S&C equation – is a popular analytical model to predict surface average C_P that has been implemented in widely used BES programs like EnergyPlus [7]. It is valid for rectangular floor-plan buildings and depends

* Corresponding author.
E-mail address: facubre@cimec.santafe-conicet.gov.ar (F. Bre).

https://doi.org/10.1016/j.enbuild.2017.11.045
0378-7788/

on two parameters: wind direction and side ratio. In the original work [6], the S&C equation was applied to a broad range of data, including buildings with different heights and roof pitch angles, yielding an acceptable correlation coefficient of 0.797. However, it needs to be improved and updated in the light of the new high-tech measurement databases. A detailed description of the low-rise S&C equation and its parameters can be found in Appendix A.

Grosso [8] proposed a set of complex parametric models in order to take into account sheltering effects, which cannot be estimated using the S&C equation. However, because of the lack of complete and high-quality experimental data, he recognized that the most useful contribution of his work may be the proposed methodology rather than the specific results. Recently, Muehleisen and Patrizi [9] developed a new parametric equation – the so-called M&P equation henceforth – to predict wind pressure coefficient for low-rise buildings. This is a simple rational equation calibrated on the based of the new, large and very detailed database of the Wind Engineering Information Center at the Tokyo Polytechnic University (TPU) [10]. The M&P equation fits very well the TPU database, with a coefficient of determination $R^2 = 0.993$. The low-rise M&P equation and its parameters are detailed in Appendix B.

Compared to the S&C equation, the M&P equation better fits not only the TPU database but also the database compiled by the Air Infiltration and Ventilation Centre (AIVC) [11]. However, the S&C equation performs better in the common case of buildings with unity depth-to-breadth ratio over a considerable range of wind attack angles ($90^\circ < \theta < 165^\circ$). So, both S&C and M&P equations have relative advantages and disadvantages depending on their application. Furthermore, neither of them can be applied to buildings with non-rectangular floor plans. Actually, up to the authors' knowledge, this is the common limitation of all the available analytical models.

To overcome such limitations, the current paper proposes a methodology to obtain a computational model satisfying three main requirements: (i) accurate prediction of C_P, (ii) valid for buildings with various floor-plan shapes (rectangular, U-shape, L-shape, etc.), and (iii) easy coupling to AFN and BPS programs.

To this end, artificial neural networks (ANN) are used to build an analytical model of the surface-average C_P for every surface of the building (walls and roofs) and for every wind attack angle. The robustness of the method is proved through its application to three low-rise rectangular building cases: flat-roofed, gable-roofed, and hip-roofed. Data for training and testing is taken from the TPU database [12]. Finally, the results obtained using the current models are compared with both S&C and M&P equations and the TPU experimental database, highlighting the accuracy of the proposed methodology to fit the experiments.

2. Methodology

This section defines the methodology proposed to develop analytical models of the surface-average C_P in low-rise buildings. Section 2.1 details the method to build and calibrate of the ANN models. Section 2.2 describes the experimental database that served to calibrate the proposed model, together with the chosen case studies.

2.1. Artificial neural networks (ANN)

An ANN is a massively parallel distributed processor made up of simple processing units that has a natural propensity for storing experimental knowledge and making it available for use in analytical way [13]. ANN is often used as a surrogate model or a response surface approximation model because of its robustness to solve multivariate and nonlinear modeling problems, like function approximations and classification.

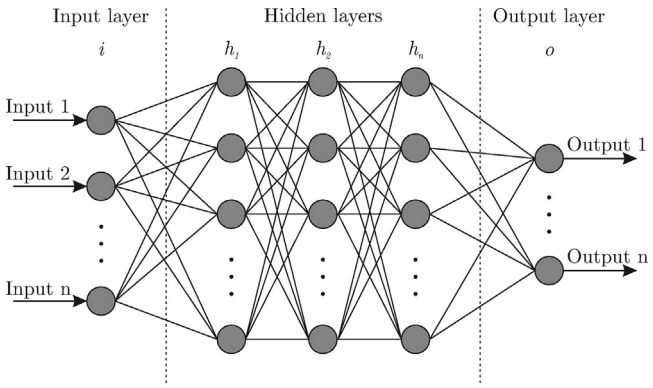

Fig. 1. Artificial neural network architecture (ANN $i - h_1 - h_2 - h_n - o$).

Some authors have used ANN to predict or interpolate C_P values. Kalogirou et al. [14] used ANN to predict C_P across the openings in a light weight single-sided naturally ventilated test room. Chen et al. [15] developed an ANN to predict C_P on gable roofs according to wind direction, roof height, and normalized roof coordinates. This work was recently extended by Gavalda et al. [16] in order to include variable plan dimensions and roof slopes as parameters. On the other hand, Fu et al. [17] developed a fuzzy neural network (FNN) approach to predict wind loads and their power spectra on a large flat roof. But, up to the authors' knowledge, neither ANN nor any other surrogate or response surface method can be found in the literature to predict C_P for every surface of a building for a wide range of input parameters.

In this work, a feed-forward multilayer ANN is used. Fig. 1 shows the general ANN architecture, which has an input layer, a set of hidden layers and an output layer. In each hidden and output layer, there are artificial neurons interconnected via adaptive weights. These weights are calibrated through a training process with input–output data. For each artificial neuron, there is an activation function, which can be any function with range $[-1, 1]$; the most common activation functions are the tangent sigmoid and the logarithmic sigmoid [13].

The definition of an ANN architecture includes determining the number of inputs, outputs, and hidden neurons, and the number of hidden layers [18]. The universal approximation theorem [19] states that a feed-forward network with a single hidden layer containing a finite number of neurons can approximate continuous functions on compact subsets of $\mathbb{R}^n$, being n the number of inputs. However, this does not mean that an ANN with one single hidden layer is optimal in terms of versatility, learning time and ease of implementation. Indeed, given the sets of input and output data, there is not a general rule to define the best ANN architecture (number of neurons and hidden layers). We propose here a method to calibrate the ANN architecture based on trial & error according to the complexity of each case. It consists of two steps: (1) a coarse calibration is made to determine the number of hidden layers, and (2) training with a increasing number of hidden neurons (starting with a few ones) until achieving the desired performance. The so-determined ANN architectures for the three considered case studies are detailed in Appendix C.

The ANN training process was made using the Levenberg–Marquardt (LM) backpropagation algorithm [20], considering the mean squared error (MSE) as convergence indicator and a maximum of 500 epochs. Let us remark that the LM method has second-order convergence rate and it was recommended by Hagan and Menhaj [21] because of its efficiency for ANN with no more that a few hundreds weights, as it is currently the case.

The previous guidelines to build an ANN models can be implemented on several computational platform such as MATLAB [22], R [23], TensorFlow [24], among others.

Now, let us apply the proposed methodology to predict the surface-average C_P on low-rise building surfaces. In this case, the ANN outputs are the surface-average C_Ps on the building surfaces, while the ANN inputs define the wind direction and building characteristics, the latter being specific for each one of the three case studies described in Section 2.2.1, giving rise to particular ANNs. The input–output data to train all these models is described below.

2.2. Databases

There are several databases containing measured C_P in building surfaces for various building geometries and a wide range of wind attack angles. The NIST aerodynamic database [25] contains time series of wind load data for low-rise gable-roofed buildings with various dimensions and terrain conditions use in the design of low-rise buildings. The database from the ASHRAE Handbook of Fundamental [26] contains the surface-average C_P for low- and high-rise buildings with rectangular floor-plan, considering four different side ratios and wind attack angles from 0° to 180° every 15°. A more detailed C_P database was compiled by the Air Infiltration and Ventilation Centre (AIVC) [27,11]. It contains tables with surface-averaged C_p for each face of rectangular low-rise buildings for wind attack angles from 0° to 180° every 45°, and for three different shielding levels: exposed, semi-sheltered and sheltered.

More recently, the Wind Engineering Information Center of the Tokyo Polytechnic University (TPU) published a comprehensive C_P database derived from a series of wind tunnel tests on a wide variety of buildings, including high-rise buildings and isolated and non-isolated low-rise buildings [12]. Given its quality and completeness, the TPU database for isolated low-rise buildings [28] will be used to train and test the ANN-based models of surface-averaged C_P in the current work. Such database contains 4176 contours of statistical values of local C_P, 700 graphs of statistical values of area-averaged C_P on the roof or the wall surfaces and time series data of point C_P for 812 test cases. The surface-averaged C_P on the building surfaces (walls and roofs) are presented as plots of mean-surface pressure for wind attack angles from 0° to 90° every 15°.

2.2.1. Case studies

The TPU database for isolated low-rise buildings [28] gives the surface-averaged C_P for all the surfaces (walls and roofs) of rectangular floor-plan buildings with either flat, gable or hip roof, see Fig. 2. Specifically, the surface-averaged C_P, say $\overline{C_P}$, is given for some values of the depth-to-breadth (or side) ratio D/B, the height-to-breadth (or height) ratio H/B, the pitch angle β (in case of gable and hip roofs) and wind attack angle θ. Note that for gable- and hip-roofed buildings, H is defined as the mean roof height. In this database, θ ranges from 0 to 90° every 15°. Since $\overline{C_P}$ is measured on all the surfaces of rectangular buildings, the upper bound of θ is easily extended to 180° considering that the $\overline{C_P}$ for θ at a given surface coincides with the $\overline{C_P}$ for the wind attack angle $180° - \theta$ at the opposite surface. In a similar way, results for the side ratio $D/B = S > 1$ and $0° \le \theta \le 90°$ can be extended to $D/B = 1/S \le 1$ taking into account that the $\overline{C_P}$ for S and wind attack angle θ at a certain surface coincides with the $\overline{C_P}$ for $1/S$ and wind attack angle $90° - \theta$ at the perpendicular surface.

Also, although $\overline{C_P}$ must be identical for opposite surfaces parallel to the wind direction, this is not the case in the TPU database because of measurements errors which may have been derived from different sources (e.g., sensor errors, nonuniform airflow through the wind tunnel, inaccuracies in the model construction or in its orientation in the wind tunnel). In these cases, a unique $\overline{C_P}$ is defined as the mean of the measured values.

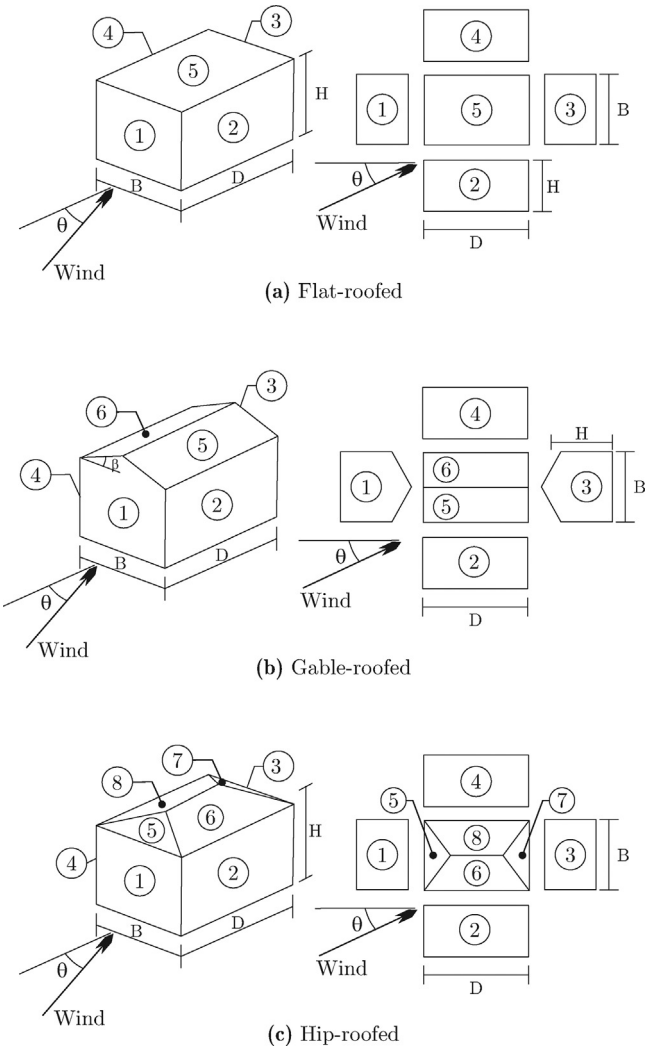

Fig. 2. Definition of the building dimensions D, B, and H, the building surfaces, the wind attack angle θ and the pitch roof angle β for the analyzed cases: (a) flat-roofed buildings, (b) gable-roofed buildings, and (c) hip-roofed buildings.

In the formulation of the S&C equation for low-rise buildings, Swami and Chandra [6] assumed $\overline{C_P}$ independent of the height ratio (H/B) and the roof angle (β). After processing the TPU database, we realized that $\overline{C_P}$ is low sensitive to the height ratio but the variation of $\overline{C_P}$ with different roof type and roof pitch angle cannot be neglected. Based on these observations, we decided to formulate a separate ANN model for each roof type, to be trained using the following data:

- *Flat-roofed buildings*: For all the walls (surfaces 1–4) and roof (surface 5), $\overline{C_P}$ is given for side ratios $D/B = 1/1, 1.5/1, 2.5/1, 1/1.5, 1/2.5$, and wind attack angles θ from 0° to 180° every 15°. This $\overline{C_P}$ is the average of the $\overline{C_P}$s for height ratios $H/B = 1/4, 2/4, 3/4, 4/4$ in the database.
- *Gable-roofed buildings*: For all the walls (surfaces 1–4) and roof (surfaces 5 and 6), $\overline{C_P}$ is given for $D/B = 1/1, 1.5/1, 2.5/1, 1/1.5, 1/2.5$, θ from 0° to 180° every 15°, and $\beta = 4.8°, 9.4°, 14°, 18.4°, 21.8°, 26.7°, 30°, 45°$. Like in the previous case, this $\overline{C_P}$ is the average of those for $H/B = 1/4, 2/4, 3/4, 4/4$ in the database. Note that the roof pitch β has been finely discretized, denoting how relevant it is.
- *Hip-roofed buildings*: For all the walls (surfaces 1–4) and roof (surfaces 5–8), $\overline{C_P}$ is given for $D/B = 1.5/1, 1/1.5$, θ from 0° to 180° every 15°, and $\beta = 26.7°, 45°$; once again, it is the average of the $\overline{C_P}$s for

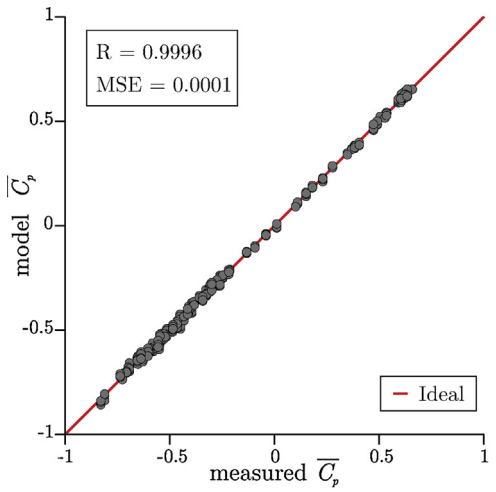

(a) Flat-roofed

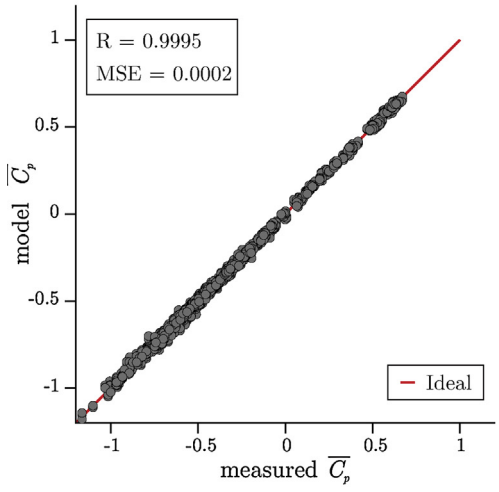

(b) Gable-roofed

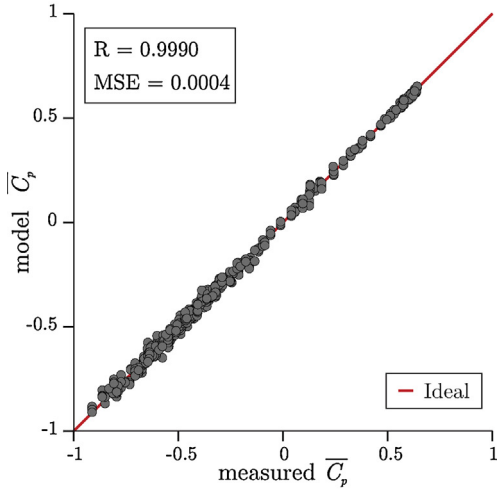

(c) Hip-roofed

Fig. 3. Fitting between the ANN outputs and the measured targets: (a) flat-roofed buildings, (b) gable-roofed buildings, and (c) hip-roofed buildings.

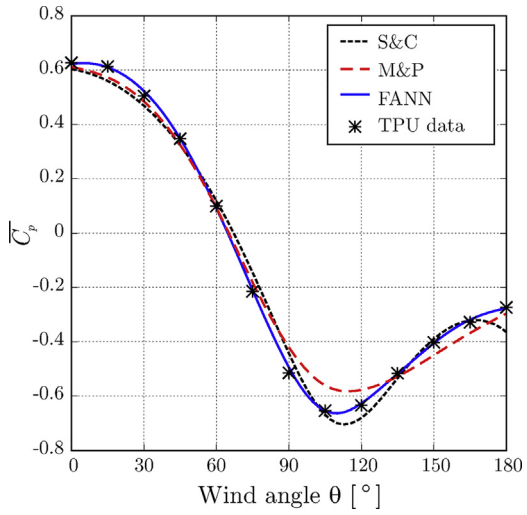

Fig. 4. Square plan flat-roofed buildings: TPU measurements vs. predictions of FANN model, the M&P and the S&C equations of the variation of the surface-averaged pressure coefficient $\overline{C_P}$ with respect to the wind attack angle θ on the surface 1.

$H/B = 1/4, 2/4, 3/4, 4/4$ in the database. In this case, the $\overline{C_P}$ is smaller than in a gable-roofed building for the same D/B, H/B, θ and β. This database is not complete enough to make a reliable model upon it, but it was included in this work in order to test the robustness of the proposed ANN-based model.

Thus, the number and the nature of inputs and outputs of the ANN models for the case studies, depending on the type of roof, are the following:

- *Flat-roofed buildings*:
  - 2 inputs: D/B, θ.
  - 5 outputs: $\overline{C_P}$ for walls (surfaces 1–4) and roof (surface 5).
- *Gable-roofed buildings*:
  - 3 inputs: D/B, β, θ.
  - 6 outputs: $\overline{C_P}$ for walls (surfaces 1–4) and roof (surface 5 and 6).
- *Hip-roofed buildings*:
  - 3 inputs: D/B, β, θ.
  - 8 outputs: $\overline{C_P}$ for walls (surfaces 1–4) and roof (surface 5–8).

Since each of these buildings have particular inputs and outputs, we formulate a separate ANN model for each case, namely the FANN, GANN and HANN models for flat-, gable- and hip-roofed buildings, respectively. Details on the formulation of each one of these models are given in Appendix C.

3. Results and discussion

First, let us evaluate the fitting between the $\overline{C_P}$s computed as outputs of the current ANN models and those from the TPU experimental database, which are the ANN targets. Fig. 3 shows the correlation between the ANN outputs and the measured $\overline{C_P}$ for the three types of roof. The fitting is excellent in all the cases: MSE = 0.0001 and correlation coefficient $R = 0.9996$ for flat-roofed buildings, MSE = 0.0002 and $R = 0.9995$ for gable-roofed buildings, and MSE = 0.0004 and $R = 0.9990$ for hip-roofed buildings.

Next, let us compare the current ANN results with those obtained using the popular S&C and M&P equations for each case.

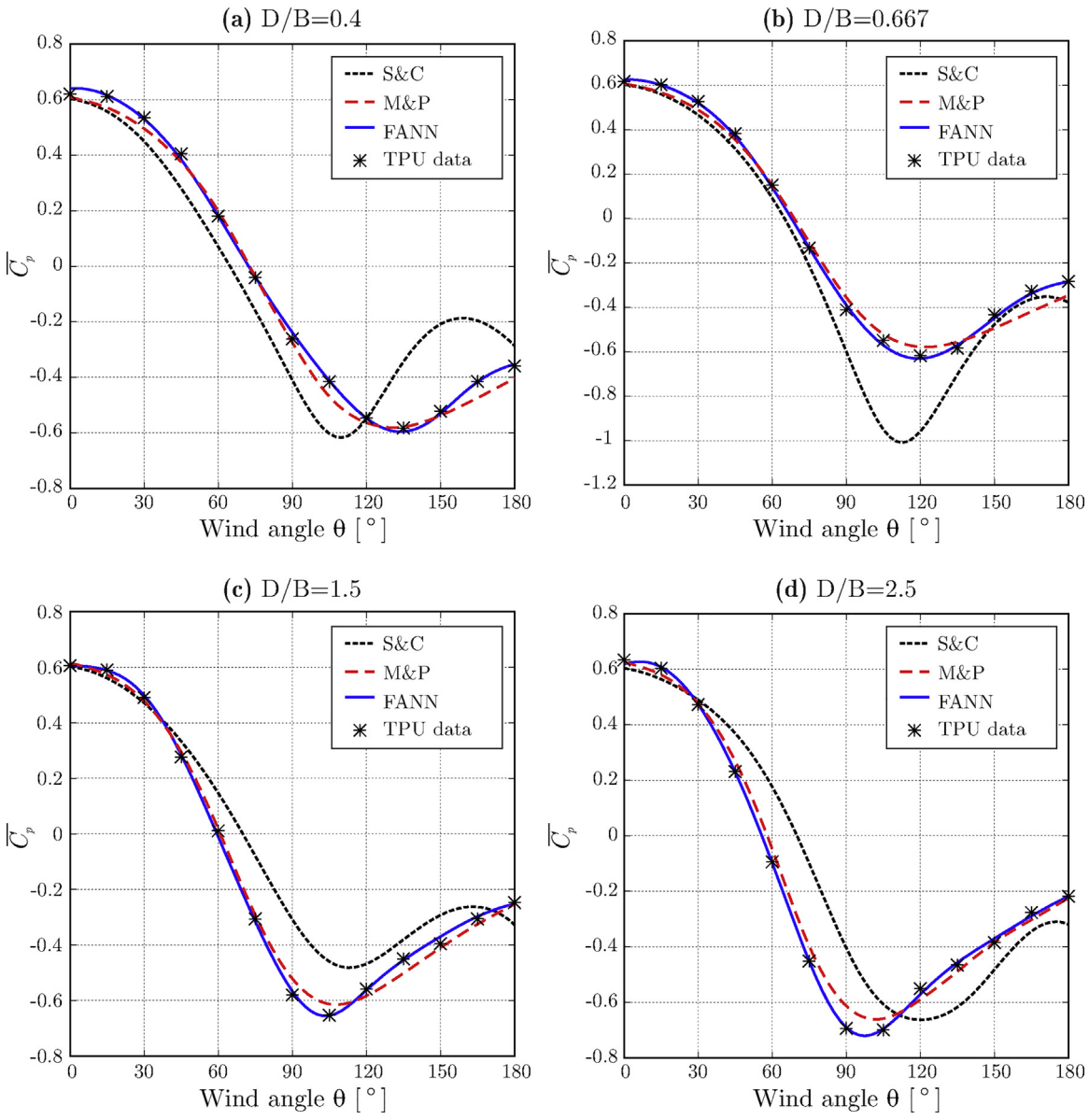

Fig. 5. Flat-roofed buildings with side ratio $D/B \neq 1$: TPU measurements vs. predictions of FANN model, the M&P and the S&C equations of the variation of the surface-averaged pressure coefficient $\overline{C_P}$ with respect to the wind attack angle θ on the surface 1.

3.1. Flat-roofed buildings

Fig. 4 shows $\overline{C_P}$ for the surface 1 (a wall) of a flat-roofed, square-plan building as a function of the wind attack angle θ. The S&C and M&P equations accurately fits for $\theta \leq 90°$; for higher θ, S&C performs usually better than M&P, as already noted by Muehleisen and Patrizzi [9]. On the other hand, FANN fits the measured TPU data with high accuracy for any θ; further, the FANN interpolation of the experimental measurements is smooth and free of overfitting. These two observations validate the chosen ANN architecture and its usefulness to predict $\overline{C_P}$ over the whole range of wind attack angles.

Fig. 5 shows $\overline{C_P}$ on surface 1 for different $D/B \neq 1$ as a function of the wind attack angle θ. As pointed out by Muehleisen and Patrizzi [9] when they proposed the M&P equation, the performance of S&C is seriously deteriorated for $D/B \neq 1$; M&P gives definitely better results for these cases. But once again, FANN exhibits the best fitting of the measured data for any D/B and θ; at the same time, it gives a smooth interpolation of the measured data.

FANN also overcomes the S&C and M&P equations as it predicts $\overline{C_P}$ for all the walls and the roof at once. Let us remind that S&C and M&P equations determine $\overline{C_P}$ for one surface at a time and are not suitable for computing $\overline{C_P}$ for the roof. As an example, Fig. 6 shows the variation of the remaining FANN outputs, i.e., $\overline{C_P}$ with respect to θ for the other walls (surfaces 2–4) and the roof (surface 5) for flat-roofed buildings with a square floor-plan. Again, there is an excellent agreement between the $\overline{C_P}$ from the TPU experimental database and that computed using FANN for any value of the wind attack angle.

3.2. Gable-roofed buildings

Fig. 7 shows the variation of $\overline{C_P}$ with respect to the wind attack angle θ for the surface 1 (a wall) of square-plan building having a gable roof with pitch angle $\beta = 45°$. In this case, S&C gives the poorest fitting of the experimental results, specially for $60° < \theta < 150°$; for instance, the difference between S&C prediction and TPU for $\theta = 90°$ is above 20%.

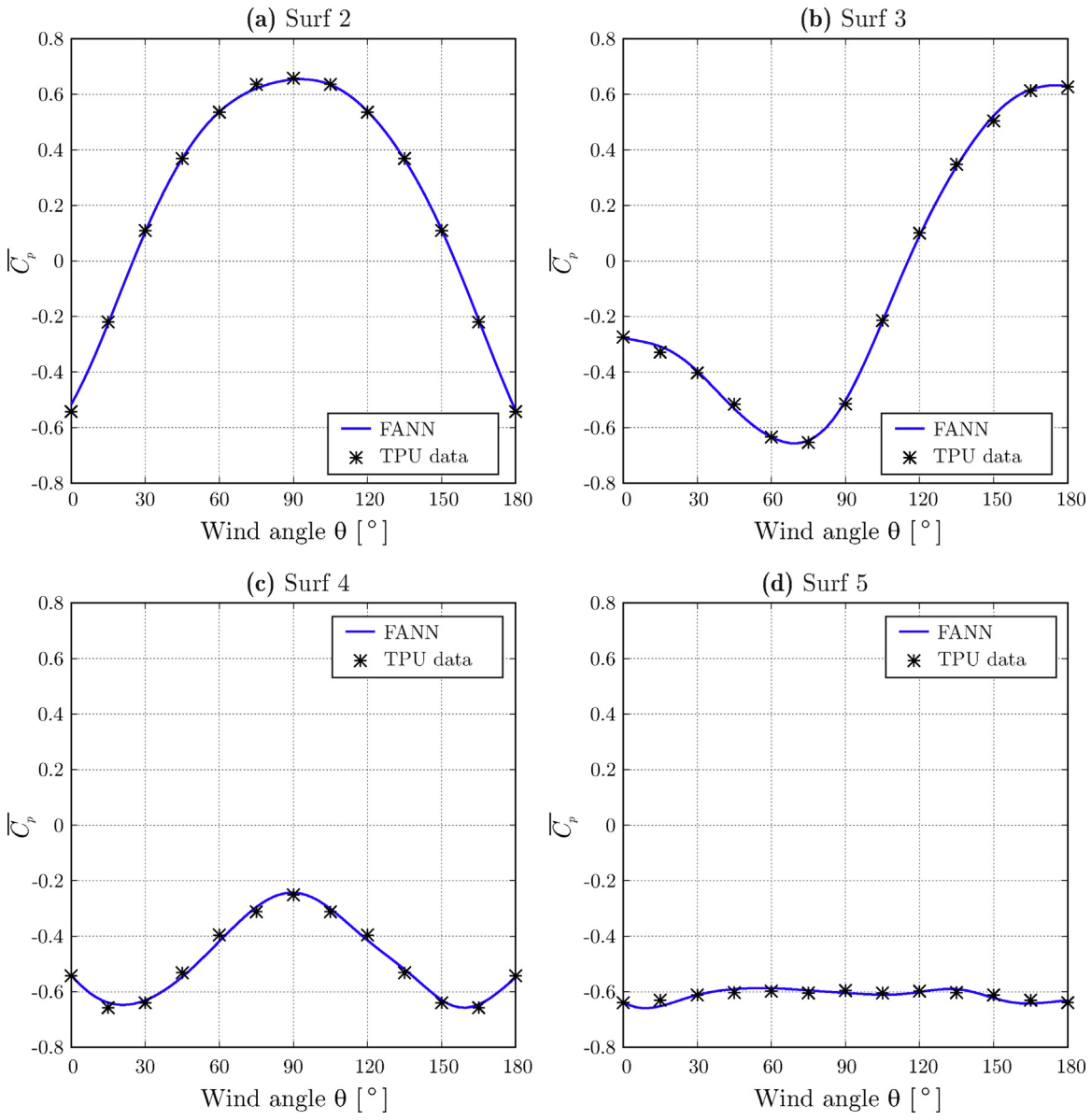

Fig. 6. Square plan flat-roofed buildings: TPU measurements vs. FANN predictions of the variation of the surface-averaged pressure coefficient $\overline{C_P}$ with respect to the wind attack angle θ for all the surfaces, except the surface 1.

On the other hand, GANN gives not only an excellent fitting but also a smooth interpolation of TPU data.

Fig. 8 shows GANN results for all the surfaces of a square-plan building with 45°-pitched gable roof. Note that these coefficients were obtained evaluating the GANN only once per incidence angle.

Let us remark that the application of S&C equation to this case carries an excessive simplification: since it depends on D/B and θ only, it gives the same $\overline{C_P}$ for walls with the same side ratio but geometrically different (as it is the case for surfaces 1 and 2, for instance). Moreover, S&C equation is not suitable for computing $\overline{C_P}$ for the roof surfaces.

3.3. Hip-roofed buildings

Fig. 9 shows the variation of $\overline{C_P}$ with respect to the wind attack angle θ for the surface 1 of buildings with a side ratio $D/B = 1.5$ and a hip roof with pitch angle $\beta = 45°$. In this case, M&P is better than S&C but it is still highly inaccurate to fit the experimental results. Meanwhile, once again, HANN gives an excellent fitting as well as a smooth interpolation of the TPU data.

Fig. 10 shows $\overline{C_P}$ as a function of θ for the surface 1 of hip-roofed buildings with side ratio $D/B = 1/1.5$, considering two roof pitch angles β: 26.7° and 45°. Besides the good agreement between HANN and TPU data for both roof pitch angles and for any wind attack angle θ, this figure highlights the differences in $\overline{C_P}$ due to the difference in the roof pitch angle, specially for $\theta > 90°$.

3.4. Accuracy of the method

In this section, the accuracy of the current ANN-based models is quantitatively assessed in the light of some examples.

Considering flat-roofed buildings with side ratio $D/B = 1.5$ and a wind attack angle $\theta = 90°$, Table 1 enables the comparison between the experimental $\overline{C_P}$ from the TPU database and the predictions given by the S&C and the M&P equations and the FANN model. While the S&C and the M&P equations are accurate enough only when they are applied to surface 2 (i.e., the windward surface),

Table 1
Flat-roofed buildings with side ratio $D/B = 1.5$: TPU measurements vs. predictions of the S&C and the M&P equations and the FANN model of the surface-averaged pressure coefficient $\overline{C_P}$ on all the building surfaces for the wind attack angle $\theta = 90^\circ$.

Surface	TPU	S&C		M&P		FANN	
	$\overline{C_P}$	$\overline{C_P}$	Error [%]	$\overline{C_P}$	Error [%]	$\overline{C_P}$	Error [%]
1	−0.580	−0.308	−46.906	−0.533	−8.154	−0.567	−2.327
2	0.618	0.604	−2.394	0.607	−1.779	0.621	0.437
3	−0.580	−0.308	−46.906	−0.533	−8.154	−0.577	−0.534
4	−0.284	−0.377	32.945	−0.345	21.728	−0.286	0.882
5	−0.727	–	–	–	–	−0.738	1.389

Table 2
Relative error comparison between the novel ANN-Model and S&C equation for gable-roofed and hip-roofed cases with $D/B = 1.5$, $\beta = 45^\circ$ and $\theta = 90^\circ$.

Roof type	Surface	TPU	S &C		ANN	
		$\overline{C_P}$	$\overline{C_P}$	Error [%]	$\overline{C_P}$	Error [%]
Gabled	1	−0.832	−0.308	−62.994	−0.82	−1.526
	2	0.604	0.604	−0.099	0.597	−1.225
	3	−0.832	−0.308	−62.994	−0.844	1.454
	4	−0.571	−0.377	−34.005	−0.589	3.169
	5	0.293	–	–	0.301	2.594
	6	−0.691	–	–	−0.698	1.100
Hipped	1	−0.667	−0.308	−53.837	−0.664	−0.513
	2	0.579	0.604	4.285	0.578	−0.178
	3	−0.667	−0.308	−53.837	−0.676	1.314
	4	−0.508	−0.377	−25.749	−0.512	0.775
	5	−0.832	–	–	−0.808	−2.826
	6	0.239	–	–	0.243	1.628
	7	−0.832	–	–	−0.797	−4.242
	8	−0.625	–	–	−0.637	2.05

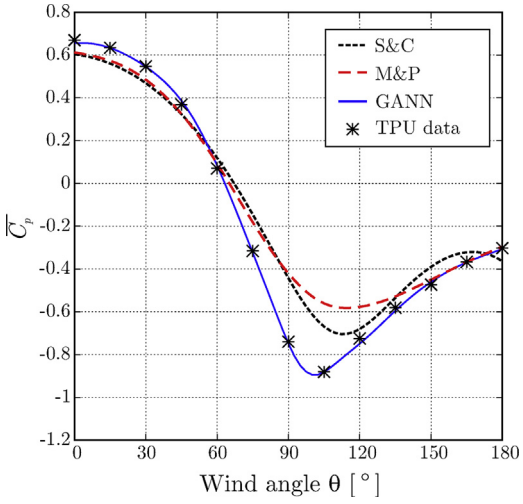

Fig. 7. Square-plan buildings with 45°-pitched gable roof: TPU measurements vs. predictions of GANN model, the M&P and the S&C equations of the variation of the surface-averaged pressure coefficient $\overline{C_P}$ with respect to the wind attack angle θ on the surface 1.

FANN is accurate enough for all the surfaces, including the roof. Actually, the maximal error magnitude using FANN is 2.3%, while it rises up to 46.9% for the S&C equation and 21.7% for the M&P equation.

Now, let us consider gable- and hip-roofed buildings and compare the respective ANN models (GANN and HANN) to the S&C equation. Note that the S&C equation was calibrated on the base not only of flat-, but also of gable- and hip-roofed buildings [6], and it is widely used for all these types of buildings; it is actually included in EnergyPlus, a popular software for building performance simulation.

Table 2 shows $\overline{C_P}$ for gable- and hip-roofed buildings having a side ratio $D/B = 1.5$ and a roof pitch angle $\beta = 45^\circ$ for a wind attack angle $\theta = 90^\circ$. Let us remind that the S&C equation does not take into account the pitch angle, which seriously affects its accuracy for buildings with pitched roof. Given the magnitude of the errors in Table 2, S&C is directly useless for all the surfaces of such pitched-roof buildings other than the windward wall. On the contrary, either GANN for gabled-roof buildings or HANN for hip-roofed ones gives good results, with errors that are always below 4.3%.

Let us remark that the performance of the proposed ANN models for the computation of $\overline{C_P}$ is equally good (actually, excellent) for flat-, gable- and hip-roofed buildings. Furthermore, they allow to predict the $\overline{C_P}$ on roofs, enabling the study of air infiltration and ventilation in case of roof apertures. Finally, note that, just modifying the ANN architecture (number of inputs and outputs, number of hidden layers and neurons therein, etc.), the proposed methodology is versatile enough to be applied to any building shape with an available database, which should be reliable enough to be used as target for training the ANN.

4. Conclusions

In this work, we proposed and developed a novel methodology based on artificial neural networks (ANN) to obtain analytical models to accurately predict the surface-averaged wind pressure coefficients in all the surfaces (walls and roofs) of low-rise buildings with different types of roofs.

Three separate ANN models were generated, the so-called FANN, GANN and HANN, addressed to flat-, gable- and hip-roofed rectangular-plan buildings, respectively. They were trained and tested taking as target the experimental database of the Wind Engineering Information Center of the Tokyo Polytechnic University (TPU).

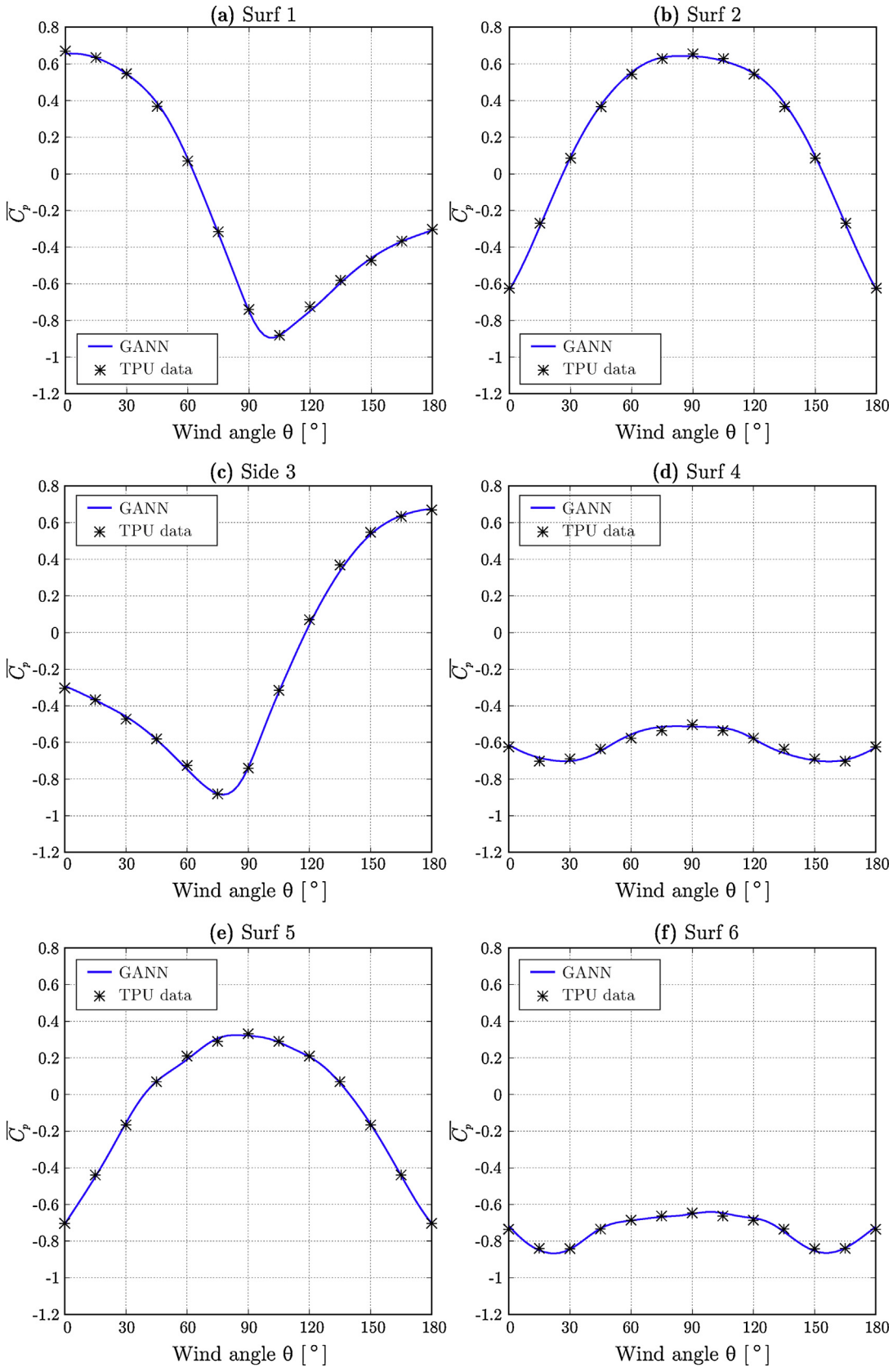

Fig. 8. Square-plan buildings with 45°-pitched gable roof: TPU measurements vs. GANN predictions of the variation of the surface-averaged pressure coefficient $\overline{C_P}$ with respect to the wind attack angle θ for all the surfaces.

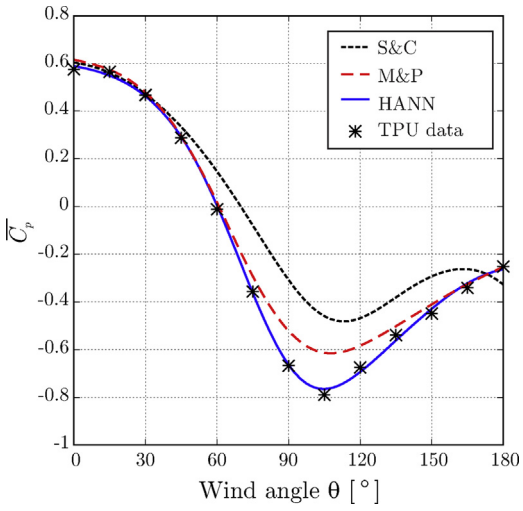

Fig. 9. Buildings with side ratio $D/B = 1.5$ and 45°-pitched hip roof: TPU measurements vs. predictions of HANN model, the M&P and the S&C equations of the variation of the surface-averaged pressure coefficient $\overline{C_P}$ with respect to the wind attack angle θ on the surface 1.

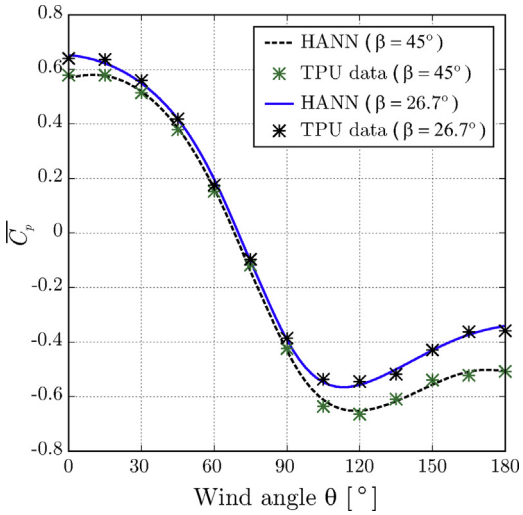

Fig. 10. Hip-roofed buildings with side ratio $D/B = 1/1.5$ and different roof pitch angles: TPU measurements vs. HANN predictions of the variation of the surface-averaged pressure coefficient $\overline{C_P}$ with respect to the wind attack angle θ on the wall surface 1.

In the lights of the results for these three types of buildings, ANN models proved to be very accurate, largely overcoming the widely used parametric equations proposed by Swami and Chandra [6], and Mueleisen and Patrizi [9]. Actually, the performance of these parametric equations, which depend on the building side ratio and the wind attack angle only, was shown to be poor in general, and even very poor for most of the surfaces of pitched-roof buildings.

Another advantage of the proposed ANN is their capacity of computing the pressure coefficients over all the building surfaces at once. Unlike the above mentioned parametric models, also the roof is considered, enabling the use of the current models in the study of phenomena like air infiltration and ventilation in presence of roof apertures.

Although it was applied here to specific buildings, the proposed methodology is amenable to be extended to buildings with an arbitrary topology (U-shape, L-shaped, etc.), including the effect of surrounding buildings, provided that you have a reliable database for training the ANN for the desired building shape and level of sheltering.

Furthermore, since the so-formulated ANN models are ultimately a closed, analytical expression of the outputs as functions of the inputs, they can be easily incorporated into softwares for building energy simulation, airflow network analysis, etc.

To ensure the accuracy of any ANN-based methodology, the ANN training has to be done with a reliable $\overline{C_P}$ database like the TPU database used in this work.

Note that the accuracy of the current models was proved for isolated buildings of three particular types and for the range of the inputs in the database used for training, otherwise it is uncertain.

Motivated by the current findings, we aim to continue this work in three main directions: (1) to embed the proposed models into EnergyPlus source code; (2) applications to low- and high-rise, isolated and non-isolated buildings with different shapes, and (3) to test the reliability of computational fluid dynamic (CFD) models to develop $\overline{C_P}$ databases of buildings with other shapes (U, L, etc.).

Acknowledgements

For funding this work, we would like to thank the Agency for Science, Technology and Innovation (SECTEI) of the Province of Santa Fe (Argentina) via the Research Project 2010-022-16 "Optimization of the Energy Efficiency of Buildings in the Province of Santa Fe".

F. Bre is a doctoral student granted by the National Scientific and Technical Research Council of Argentina (CONICET).

Appendix A. Swami and Chandra (S&C) equation

The S&C equation [6] defines the surface-average wind pressure coefficient at a wall of a low-rise building as

$$\overline{C_P}(\theta, D/B) = \overline{C_P}(0^\circ)\ln[1.248\ -0.703\sin\theta/2) - 1.175\sin^2(\theta) + 0.131\sin^3(2G\theta) + 0.769\cos(\theta/2)! + !0.07G^2\sin^2(\theta/2) + 0.717\cos^2(\theta/2)],$$

where θ is the wind attack angle on the surface, and $G = \ln(D/B)$ is the natural logarithm of the side ratio D/B, and $\overline{C_P}(0^\circ)$ is the $\overline{C_P}$ for $\theta = 0^\circ$, assumed by Swami and Chandra to be equal to 0.6 independently of D/B.

Appendix B. Muehleisen and Patrizi (M&P) equation

The M&P equation [9] defines the surface-average wind pressure coefficient at a wall of a low-rise building using the following rational function of the wind attack angle θ and the side ratio D/B:

$$\overline{C_P}(\theta, D/B) = \frac{a_0 + a_1 G + a_2\theta + a_3\theta^2 + a_4 G\theta}{1 + b_1 G + b_2\theta + b_3\theta^2 + b_4 G\theta}, \quad \text{with } G = \ln(D/B),$$

where a_i and b_i are adjustable coefficients. Muehleisen and Patrizi calibrated them using non-linear curve fitting on the base of the TPU database for low-rise buildings [28], obtaining $a_0 = 6.12 \times 10^{-1}$, $a_1 = -1.78 \times 10^{-1}$, $a_2 = -1.15 \times 10^{-2}$, $a_3 = 3.28 \times 10^{-5}$, $a_4 = 1.67 \times 10^{-3}$, $b_1 = -3.12 \times 10^{-1}$, $b_2 = -1.59 \times 10^{-2}$, $b_3 = 9.82 \times 10^{-5}$, $b_4 = 2.15 \times 10^{-3}$. Note that in the original paper [9], b_2 has a typo mistake; we fixed it after communication with Muehleisen.

Appendix C. Formulation of the ANN models

In this section, is given a detailed information to implement the ANN models developed. These ANN models are available in doi:10.17632/mj6s6x37vm.3

An ANN is a set of unit cells (or artificial neurons) arranged in an input layer, one or more hidden layers, and an output layer. Each neuron is connected to those neurons in the neighboring layers via

Table 3
Parameters of the ANN models.

Parameter	FANN	GANN	HANN
Inputs	D/B, θ	D/B, β, θ	D/B, β, θ
Outputs	$\overline{C_P}$ on surfaces 1–5	$\overline{C_P}$ on surfaces 1–6	$\overline{C_P}$ on surfaces 1–8
Architecture(I-H-···-O)	2-9-8-5	3-20-20-6	3-20-8

Table 4
Minimum and maximum inputs and outputs for the ANN models.

	Parameter	FANN		GANN		HANN	
		Min.	Max.	Min.	Max.	Min.	Max.
Inputs	D/B	0.4	2.5	0.4	2.5	0.667	1.5
	β			4.8°	45°	26.7°	45°
	θ	0°	180°	0°	180°	0°	180°
Outputs	$\overline{C_P}$ Surf. 1	−0.6995	0.6334	−0.9610	0.6695	−0.7892	0.6403
	$\overline{C_P}$ Surf. 2	−0.6939	0.6581	−0.9516	0.6687	−0.6672	0.6403
	$\overline{C_P}$ Surf. 3	−0.6995	0.6334	−0.961	0.6695	−0.7892	0.6403
	$\overline{C_P}$ Surf. 4	−0.6995	−0.2179	−0.961	−0.1934	−0.7892	−0.2116
	$\overline{C_P}$ Surf. 5	−0.8304	−0.3000	−1.1645	0.3315	−0.9127	0.1291
	$\overline{C_P}$ Surf. 6			−1.1645	0.2947	−0.8640	0.2422
	$\overline{C_P}$ Surf. 7					−0.9127	0.1291
	$\overline{C_P}$ Surf. 8					−0.8640	0.2422

Table 5
Weights and bias values for FANN.

Layer k	Neuron j	b_j^k	w_{1j}^k	w_{2j}^k	w_{3j}^k	w_{4j}^k	w_{5j}^k	w_{6j}^k	w_{7j}^k	w_{8j}^k	w_{9j}^k
H1	1	6.89	−5.57	1.43							
	2	−1.13	0.74	−1.35							
	3	2.02	−2.98	−1.36							
	4	1.85	0.33	2.01							
	5	0.98	−1.09	1.57							
	6	0.26	−0.17	−1.56							
	7	−1.89	0.58	2.41							
	8	2.24	2.34	−2.23							
	9	−4.96	−6.16	−0.39							
H2	1	0.50	3.87	−2.42	−0.02	−3.14	−1.76	2.45	0.85	−0.42	0.24
	2	0.93	−1.03	−0.81	0.01	−0.57	−0.62	−0.59	−0.67	0.18	−0.04
	3	−11.47	3.78	1.05	0.78	8.02	−5.28	−6.35	−1.39	0.14	0.05
	4	−4.12	1.35	−14.32	1.30	−2.19	−8.91	−1.29	1.73	0.17	0.01
	5	1.86	−0.66	−0.54	−1.08	0.17	−0.40	−0.70	0.69	0.53	−0.15
	6	−2.53	2.53	4.85	0.12	1.27	1.61	−1.97	0.33	−0.10	0.03
	7	−0.22	2.81	3.42	−0.32	−1.29	2.07	0.77	−0.43	−0.25	0.05
	8	2.01	1.21	1.33	0.07	0.76	1.10	−1.80	1.92	−0.03	0.14
O	1	1.21	−0.83	0.08	0.18	0.42	0.45	1.45	2.71	−0.07	
	2	−2.87	0.11	−4.20	0.15	−0.44	0.46	−5.97	−2.58	−1.00	
	3	0.12	0.01	−4.43	0.24	−0.57	−1.92	−4.86	−6.93	−3.51	
	4	2.31	−1.62	4.44	−2.19	−3.37	−2.09	6.63	−0.72	2.47	
	5	1.22	−2.33	−6.11	−0.98	−3.93	−3.58	−4.60	−9.43	−3.74	

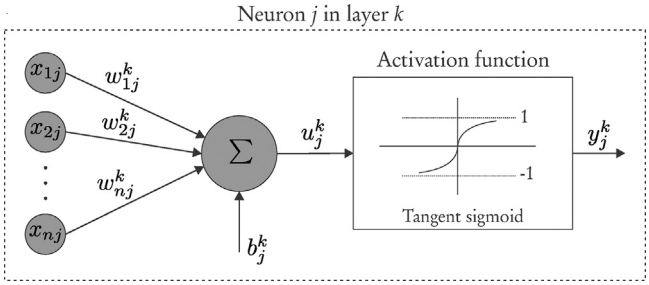

Fig. 11. Model of the neuron j in layer k.

adaptive weights. Fig. 11 shows the model of a generic neuron j in the hidden layer k, whose output is defined as follows:

$$y_j^k = f\left(\sum_{i=1}^{n} w_{ij}^k x_i^k + b_j^k\right),$$

where w_{ij}^k is the weight of the connection between the ith neuron of the previous layer and the considered neuron, x_i^k is the input from ith neuron of the previous layer, b_j^k is the bias associated with the current neuron, and f is the activation function. Here, we adopt the tangent sigmoid $f(u) = -1 + 2/(1 + e^{-2u})$ for the hidden layers, and the linear function $f(u) = u$ for the output later.

Table 3 gives the inputs, the outputs and the architecture (i.e., the number of layers and neurons per layer) for the three ANN models.

Table 6
Weights and bias values for GANN.

L. k	N. j	b_j^k	w_{1j}^k	w_{2j}^k	w_{3j}^k	w_{4j}^k	w_{5j}^k	w_{6j}^k	w_{7j}^k	w_{8j}^k	w_{9j}^k	w_{10j}^k	w_{11j}^k	w_{12j}^k	w_{13j}^k	w_{14j}^k	w_{15j}^k	w_{16j}^k	w_{17j}^k	w_{18j}^k	w_{19j}^k	w_{20j}^k
H1	1	−2.69	1.37	−0.02	2.17																	
	2	1.58	−0.18	1.28	−1.24																	
	3	−1.38	0.28	−1.22	1.06																	
	4	−0.73	1.16	0.89	−0.22																	
	5	−1.73	0.02	−0.03	−1.92																	
	6	−1.34	−0.13	−0.76	−3.94																	
	7	0.99	−0.16	−0.09	1.65																	
	8	0.07	1.07	−0.38	−0.80																	
	9	0.33	−1.06	0.02	−0.86																	
	10	0.71	0.22	−2.25	−1.77																	
	11	0.11	0.24	−0.02	1.22																	
	12	−0.76	−0.62	1.82	−1.45																	
	13	0.49	1.46	−0.08	−1.53																	
	14	−0.56	−0.28	−1.93	−0.48																	
	15	−3.76	−4.13	0.02	−1.35																	
	16	−1.44	0.17	−0.01	2.07																	
	17	2.06	2.53	0.01	0.47																	
	18	4.76	5.64	0.19	−1.40																	
	19	9.32	0.23	−7.48	−6.25																	
	20	−6.30	−6.75	−0.18	0.17																	
H2	1	−11.11	−0.90	−1.83	−3.12	0.20	−8.39	0.20	−1.68	−0.04	1.25	−0.28	5.93	−0.05	1.61	0.94	3.06	−7.01	−2.39	−2.28	0.06	−2.94
	2	1.01	−10.77	0.09	−0.36	−0.16	−0.37	0.06	−0.15	−0.29	0.28	−0.06	1.37	−0.06	0.84	−0.08	−0.17	11.69	−0.03	−0.33	−0.04	0.07
	3	2.53	−9.09	−1.14	−1.52	−0.22	−0.16	0.22	−0.28	−0.48	0.40	−0.08	2.39	−0.07	0.81	−0.09	−0.06	9.38	0.56	−0.77	−2.00	−0.16
	4	−1.44	−0.06	−0.93	−1.00	0.12	0.24	0.99	−0.27	0.19	−0.22	0.03	3.86	0.09	−0.21	−0.07	0.27	0.12	−2.69	0.18	0.04	−1.04
	5	0.64	−0.36	0.83	0.78	0.06	−0.25	−0.20	−0.30	0.08	−0.24	0.02	−1.54	0.02	−0.02	0.03	0.04	0.16	0.36	−0.05	0.01	−0.02
	6	0.04	0.27	−1.13	−1.00	−0.16	−0.04	0.16	−0.52	−0.22	0.11	−0.02	1.21	−0.06	0.25	−0.05	−0.36	−0.08	−0.46	−0.21	−0.02	−0.19
	7	0.03	0.01	0.34	0.10	0.14	1.26	−0.15	1.46	0.53	−0.27	−0.04	−0.76	0.03	−0.62	0.05	0.21	−0.34	0.45	0.05	−0.02	0.08
	8	−0.24	−8.61	−2.94	0.28	2.24	−2.19	0.36	1.56	8.03	6.45	−0.99	3.05	0.45	−2.86	0.68	−4.44	7.48	−8.15	6.12	0.72	4.85
	9	−1.08	0.07	−0.86	−1.18	−0.29	0.45	−0.11	1.27	−1.91	−1.20	0.14	−0.51	0.31	1.39	0.55	−0.63	0.58	−3.07	0.12	0.33	−1.12
	10	7.67	−0.60	0.32	0.49	−0.12	0.77	0.10	0.84	−0.07	−0.16	−0.06	−0.97	−0.17	0.52	−0.01	0.19	0.39	−0.96	−0.19	−0.09	5.81
	11	0.23	−0.51	1.03	0.95	0.11	0.96	−0.05	0.28	0.21	0.04	0.01	−0.31	0.03	−0.14	0.01	0.15	0.57	−0.06	0.17	−0.01	0.12
	12	6.82	−1.56	3.69	3.88	0.26	−2.41	−0.05	−10.41	0.11	2.12	−0.02	2.94	−0.07	1.02	−0.03	−0.71	1.03	−3.19	1.59	−0.01	1.75
	13	1.80	0.08	−1.76	−1.11	−0.19	2.51	0.12	0.53	1.35	0.05	−0.19	−1.23	−0.21	−0.84	−0.41	−1.05	−0.59	1.71	−0.83	−0.16	0.72
	14	0.20	1.29	−3.80	−4.10	−0.26	11.65	−0.02	12.03	−0.09	−1.88	0.06	−1.74	0.17	−0.75	0.06	0.17	−1.04	2.27	−1.28	0.08	−1.34
	15	−0.46	0.16	1.45	1.46	0.31	−1.01	0.28	−1.42	−0.74	0.80	0.23	2.46	0.33	0.25	0.11	1.69	−0.26	1.48	1.06	0.26	0.50
	16	1.12	0.18	−2.85	−2.83	−0.05	−0.56	0.27	−1.70	0.57	0.43	−0.06	1.62	−0.04	−0.12	−0.08	−0.14	0.18	0.04	−0.41	−0.03	−0.30
	17	−2.56	0.79	−1.15	−1.13	−0.09	−0.60	0.01	−0.64	0.18	−0.22	−0.04	−0.88	−0.07	0.16	−0.01	−0.46	−2.84	−0.38	−0.32	−0.13	−0.31
	18	10.31	−0.83	4.72	4.80	0.28	−0.47	−1.24	1.26	−0.30	−0.38	0.24	−3.25	0.15	0.11	−0.07	−0.38	1.69	−0.46	1.99	0.10	12.10
	19	1.18	−0.15	−0.51	−0.33	0.27	0.32	0.04	−0.39	1.71	0.80	−0.10	−0.14	−0.16	−1.17	−0.37	0.25	−0.22	2.21	−0.16	−0.18	0.95
	20	−6.65	1.52	4.89	3.76	−1.26	−0.66	0.00	2.62	0.02	−2.10	−1.91	−3.44	0.98	−0.09	1.75	−4.99	−1.18	2.72	−3.22	0.14	1.39
O	1	2.04	−0.02	−0.42	0.05	1.22	−1.54	−2.08	−0.95	0.01	0.29	0.27	0.10	2.83	−0.04	3.30	−0.03	−0.30	0.82	−0.14	0.48	−0.32
	2	−2.90	−0.04	−1.06	0.26	−2.87	−0.88	−1.32	0.49	0.00	0.19	0.56	−2.09	−0.30	−0.07	−0.26	0.02	0.17	−0.13	0.19	0.34	0.13
	3	−0.04	−0.04	1.33	−0.17	−2.17	−3.05	1.57	1.67	0.01	0.26	1.50	0.82	−2.29	−0.25	−1.86	0.75	−0.70	2.59	0.37	0.70	0.16
	4	9.58	0.44	−2.67	2.31	6.08	−2.20	1.07	2.18	−0.03	−0.22	0.87	0.02	0.49	0.95	0.84	1.07	−2.53	2.66	−0.19	−0.76	−0.88
	5	−4.38	−0.06	−7.09	3.84	−8.06	−0.21	−5.39	−5.50	−0.12	1.77	−4.24	−0.48	−0.41	−0.30	−0.11	−2.81	0.94	−3.00	0.25	1.75	1.16
	6	−0.05	−0.02	2.30	−1.03	−0.32	−8.37	−15.15	−3.04	−0.21	−5.55	−0.56	1.42	−0.67	2.51	−0.58	−1.55	2.62	−4.53	−1.19	−10.17	0.69

Table 7
Weights and bias values for HANN.

L. k	N. j	b_j^k	w_{1j}^k	w_{2j}^k	w_{3j}^k	w_{4j}^k	w_{5j}^k	w_{6j}^k	w_{7j}^k	w_{8j}^k	w_{9j}^k	w_{10j}^k	w_{11j}^k	w_{12j}^k	w_{13j}^k	w_{14j}^k	w_{15j}^k	w_{16j}^k	w_{17j}^k	w_{18j}^k	w_{19j}^k	w_{20j}^k
H1	1	1.09	−0.10	−0.40	0.96																	
	2	1.43	0.10	1.29	−1.64																	
	3	0.69	−0.11	−0.01	−0.80																	
	4	4.51	−0.07	−3.98	2.59																	
	5	−2.18	6.59	2.97	−6.17																	
	6	1.92	−5.49	4.37	−4.49																	
	7	−0.34	−0.08	−1.15	−0.96																	
	8	0.43	0.12	−0.10	−2.70																	
	9	0.43	0.15	−0.32	−1.29																	
	10	−0.45	−0.18	0.08	−2.74																	
	11	−0.09	−1.22	−0.01	0.05																	
	12	−0.36	−0.07	0.82	−0.83																	
	13	1.59	0.11	1.21	−2.44																	
	14	−0.74	0.11	2.81	−1.99																	
	15	0.72	0.20	−0.70	1.25																	
	16	2.11	−0.10	−1.87	2.03																	
	17	−3.77	−0.13	−3.96	1.33																	
	18	−1.34	−0.12	0.03	−1.50																	
	19	−24.70	−21.89	0.37	−19.45																	
	20	5.65	1.51	4.05	1.34																	
O	1	0.16	1.09	−0.76	0.42	1.05	−0.03	−0.03	0.05	−1.01	−0.54	1.12	−0.23	−1.34	1.12	−0.64	−0.54	−2.69	−0.54	0.49	−0.01	−0.07
	2	−2.03	2.10	4.61	1.02	−1.49	0.01	0.01	1.51	0.15	−0.04	−0.02	−0.44	2.00	−2.04	1.34	0.01	1.98	3.43	−1.62	0.02	0.01
	3	−1.14	−0.74	−1.21	2.99	−0.59	−0.03	−0.01	−2.31	−1.22	0.15	0.34	−0.12	−3.95	0.42	0.04	−0.61	0.62	−1.01	0.96	−0.01	−0.08
	4	8.64	1.77	34.64	−9.34	−13.16	0.11	0.03	12.52	6.71	−10.02	−0.80	−1.87	28.28	−16.45	1.87	4.71	19.97	25.59	−1.23	−0.03	0.42
	5	14.60	2.68	5.35	−18.81	4.22	−0.24	−0.24	26.05	−4.72	−11.23	−0.74	−1.87	36.63	4.89	−9.45	0.47	−12.66	5.30	−12.86	−0.27	−0.77
	6	6.50	−6.50	−34.06	−13.17	0.79	−0.31	−0.30	6.30	−0.05	7.22	0.02	2.10	3.56	10.28	2.37	2.68	0.38	−24.81	−6.97	−0.32	−1.39
	7	−12.02	−3.93	16.18	20.03	−17.94	0.01	0.05	−19.96	9.30	2.52	1.12	−0.41	−34.71	−16.58	16.37	−4.99	32.15	9.08	10.47	0.04	0.08
	8	−8.92	13.89	29.56	16.98	−7.89	0.36	0.21	−9.17	2.16	−8.21	−0.77	−2.58	9.10	−9.36	−5.49	6.73	5.98	23.91	13.29	0.27	1.13

The inputs x and the outputs y are linearly normalized as follows:

$$x_n = 2\frac{x - x_{\min}}{x_{\max} - x_{\min}} - 1, \qquad y_n = 2\frac{y - y_{\min}}{y_{\max} - y_{\min}} - 1, \tag{1}$$

where x_{min}, x_{max}, y_{min} and y_{max} for each ANN model are given in Table 4.

Finally, Tables 5–7 give the results of training (i.e., the weights and biases) for FANN, GANN and HANN, respectively.

References

[1] A. Rackes, M.S. Michael, Alternative ventilation strategies in U.S. offices: comprehensive assessment and sensitivity analysis of energy saving potential, Build. Environ. 116 (2017) 30–44.
[2] R. Ramponi, A. Angelotti, B. Blocken, Energy saving potential of night ventilation: sensitivity to pressure coefficients for different European climates, Appl. Energy 123 (2014) 185–195.
[3] D. Coŝtola, B. Blocken, J.L.M. Hensen, Overview of pressure coefficient data in building energy simulation and airflow network programs, Build. Environ. 44 (10) (2009) 2027–2036.
[4] M.V. Swami, S. Chandra, Procedures for calculating natural ventilation airflow rates in buildings, in: ASHRAE Final Report FSEC-CR-163-86. ASHRAE Research Project, 1987.
[5] D. Cóstola, B. Blocken, M. Ohba, J.L.M. Hensen, Uncertainty in airflow rate calculations due to the use of surface-averaged pressure coefficients, Energy Build. 42 (6) (2010) 881–888.
[6] M.V. Swami, S. Chandra, Correlations for pressure distribution on buildings and calculation of natural-ventilation airflow, ASHRAE Trans. 94 (3127) (1988) 243–266.
[7] D.B. Crawley, L.K. Lawrie, F.C. Winkelmann, W.F. Buhl, Y.J. Huang, C.O. Pedersen, R.K. Strand, R.J. Liesen, D.E. Fisher, M.J. Witte, et al., EnergyPlus: creating a new-generation building energy simulation program, Energy Build. 33 (4) (2001) 319–331.
[8] M. Grosso, Wind pressure distribution around buildings: a parametrical model, Energy Build. 18 (2) (1992) 101–131.
[9] R.T. Muehleisen, S. Patrizi, A new parametric equation for the wind pressure coefficient for low-rise buildings, Energy Build. 57 (2013) 245–249.
[10] Y. Quan, Y. Tamura, M. Matsui, S. Cao, A. Yoshida, TPU aerodynamic database for low-rise buildings, 12th International Conference on Wind Engineering (2007) 2–6, URL http://www.wind.arch.t-kougei.ac.jp/info_center/windpressure/lowrise/mainpage.html.
[11] M. Orme, N. Leksmono, AIVC Guide 5: Ventilation Modelling Data Guide, International Energy Agency, Air Infiltration Ventilation Center. AIC-GUI, 5, 2002.
[12] Tokyo Polytechnic University (TPU), TPU Aerodynamic Database, Global Center of Excellence Program, Tokyo Polytechnic University, Tokyo, Japan, 2017, URL http://wind.arch.t-kougei.ac.jp/system/eng/contents/code/tpu.
[13] S.S. Haykin, 2009. Neural Networks and Learning Machines, vol. 3, Pearson Upper Saddle River, NJ, USA.
[14] S. Kalogirou, M. Eftekhari, L. Marjanovic, Predicting the pressure coefficients in a naturally ventilated test room using artificial neural networks, Build. Environ. 38 (3) (2003) 399–407.
[15] Y. Chen, G.A. Kopp, D. Surry, Prediction of pressure coefficients on roofs of low buildings using artificial neural networks, J. Wind Eng. Ind. Aerodyn. 91 (3) (2003) 423–441.
[16] X. Gavalda, J. Ferrer-Gener, G.A. Kopp, F. Giralt, Interpolation of pressure coefficients for low-rise buildings of different plan dimensions and roof slopes using artificial neural networks, J. Wind Eng. Ind. Aerodyn. 99 (5) (2011) 658–664.
[17] J.Y. Fu, Q.S. Li, Z.N. Xie, Prediction of wind loads on a large flat roof using fuzzy neural networks, Eng. Struct. 28 (1) (2006) 153–161.
[18] J. Daniel, Fonseca, O. Daniel, Navaresse, G.P. Moynihan, Simulation metamodeling through artificial neural networks, Eng. Appl. Artif. Intell. 16 (3) (2003) 177–183.
[19] B.C. Csáji, 2001. Approximation with Artificial Neural Networks, vol. 24, Faculty of Sciences, Etvs Lornd University Hungary, 48.
[20] D.W. Marquardt, An algorithm for least-squares estimation of nonlinear parameters, J. Soc. Ind. Appl. Math. 11 (2) (1963) 431–441.
[21] M.T. Hagan, M.B. Menhaj, Training feedforward networks with the Marquardt algorithm, IEEE Trans. Neural Netw. 5 (6) (1994) 989–993.
[22] S. Fritsch, F. Guenther, M.F. Guenther, Package "neuralnet", 2016.
[23] H. Demuth, M. Beale, Neural Network Toolbox for Use with MATLAB-User's Guide Version 3.0., 1993.
[24] M. Abadi, A. Agarwal, P. Barham, E. Brevdo, Z. Chen, C. Citro, G.S. Corrado, A. Davis, J. Dean, M. Devin, et al., Tensorflow: Large-Scale Machine Learning on Heterogeneous Distributed Systems, 2016, , URL https://www.tensorflow.org/ arXiv:1603.04467.
[25] T.C.E. Ho, D. Surry, D. Morrish, G.A. Kopp, The two contribution to the NIST aerodynamic database for wind loads on low buildings: Part 1. Archiving format and basic aerodynamic data, J. Wind Eng. Ind. Aerodyn. 93 (1) (2005) 1–30.
[26] Handbook, ASHRAE and others. Fundamentals, vol. 111 American Society of Heating, Refrigerating and Air Conditioning Engineers Atlanta 2001.
[27] M.W. Liddament, Air Infiltration Calculation Techniques: An Applications Guide, Air Infiltration and Ventilation Centre Berkshire, UK, 1986.
[28] Tokyo Polytechnic University (TPU), Aerodynamic Database for Low-Rise Buildings, 2017, URL http://www.wind.arch.t-kougei.ac.jp/info_center/windpressure/lowrise.